

Glancing-incidence x-ray fluorescence of layered materials

D. K. G. de Boer

Philips Research Laboratories, P.O. Box 80000, 5600JA Eindhoven, The Netherlands

(Received 2 January 1991)

X-ray fluorescence spectroscopy normally probes the first few micrometers of a material, but under conditions of glancing incidence the surface sensitivity is enlarged to the nanometer regime. In this paper, a formalism is given for the calculation of x-ray fluorescence intensities that is also valid at glancing incidence and includes absorption and enhancement effects. Calculations based on this theory for the angular dependence of glancing-incidence x-ray fluorescence (GIXF) intensities compare well with experimental data. Standing waves in thin layers are shown to be a sensitive probe for elements at various depths, an effect that can be exploited in GIXF for depth profiling in layered materials.

I. INTRODUCTION

If x rays impinge on a flat material under a small glancing angle, a large variety of physical phenomena can occur, such as total reflection,¹ interference fringes from a layer on a substrate,² and Bragg diffraction from a periodic multilayer.^{3,4} As the penetration depth of the x rays changes from the micrometer to the nanometer region, if the critical angle for total reflection is passed,⁵ x-ray measurements in the glancing-incidence region can yield information about the upper layers of flat specimens. Techniques which make use of this effect are x-ray reflectivity,^{2,5} glancing-incidence x-ray photoelectron spectroscopy,⁶ glancing-incidence x-ray absorption spectroscopy,⁷ glancing-incidence x-ray diffraction (GIXD) or scattering (GIXS),⁸ and glancing-incidence x-ray fluorescence (GIXF), with which this paper deals. Since it is often possible to combine two or more of these techniques, the acronym GIXA (glancing-incidence x-ray analysis) is proposed for this combination.

The first way in which GIXF was used was after it was realized⁹ that if a small amount of material on top of a flat substrate is analyzed at glancing incidence, background radiation due to substrate scattering is considerably reduced. This is the basis of total-reflection x-ray fluorescence (TXRF) as a method for chemical analysis of small quantities¹⁰ and of contamination on semiconductor wafers.^{11,12} Later, the angular dependence of GIXF was used to obtain information on composition as a function of depth.^{13,14} This method has been used to investigate impurity profiles in semiconductors,^{11,15,16} periodic multilayers,⁴ and very thin^{11,17,18} and thicker layers on a substrate,^{17,19,20} as well as adsorbed molecules.^{21,22}

The aim of the present paper is twofold: to give a complete theory for GIXF, in which gaps in previous formulations are filled, and to show the potentialities of GIXF for depth analysis of layered materials, especially using interference fringes. Section II deals with the theory for the calculation of GIXF intensities. The incident wave field is described using macroscopic optical theory.^{5,23} Compared with previous formulations,^{6,18,24} ambiguities are resolved, and for the first time absorption and fluores-

cence enhancement in the glancing-incidence regime are treated. In principle, the theory is valid for soft x rays too. The approximations which can be used for harder x rays are discussed. In Sec. III the theory is applied to calculate GIXF intensities of layered materials. It is found that, using standing-wave conditions just above the critical angle, a surprising sensitivity for elements in different layers can be obtained. In Sec. IV a comparison is made with experiments,²⁵ and it is shown that in many cases it is possible to determine depth distributions from GIXF measurements. In Sec. V a final discussion of the results is given, and the method is compared with other techniques.

II. THEORY

A. Reflection and refraction

In order to calculate x-ray fluorescence (XRF) intensities, the electromagnetic field everywhere in the material has to be known. A plane electromagnetic wave in medium j at position \mathbf{r} can be written as $\mathbf{E}_j = \mathbf{E}_j^0 \exp[i(\omega t - \mathbf{k}_j \cdot \mathbf{r})]$. The wave vector can be expressed as $\mathbf{k}_j = (2\pi/\lambda)\mathbf{N}_j$, where λ is the wavelength of the incoming radiation and $\mathbf{N}_j = \mathbf{N}_j' - i\mathbf{N}_j''$ is the complex *vector of refraction*.²⁶ Note that \mathbf{N}_j' is perpendicular to the planes of equal phase, whereas \mathbf{N}_j'' is perpendicular to the planes of equal amplitude. Below, a third vector, that of energy flow, will be encountered.

From Maxwell's equations it can be shown²⁶ that $\mathbf{N}_j \cdot \mathbf{N}_j = \epsilon_j$, where $\epsilon_j = \epsilon_j' - i\epsilon_j''$ is the complex dielectric constant^{1,27} of material j .

It is common to use a refractive index $n_j = 1 - \delta_j - i\beta_j$, where both δ_j and β_j are of the order of 10^{-6} . Assuming that this expression is valid if \mathbf{N}_j' and \mathbf{N}_j'' are parallel,²⁶ one obtains $\epsilon_j = n_j^2$ and thus, in good approximation, $\epsilon_j' \approx 1 - 2\delta_j$ and $\epsilon_j'' \approx 2\beta_j$.

Next, consider a multiple thin-film sample, such as in Fig. 1. In layer j the vector of refraction is \mathbf{N}_j . If "layer" 0, the medium for the incident beam, is vacuum with $\epsilon_0 = 1$ (or air, $\epsilon_0 \approx 1$) and if all interfaces are parallel, one

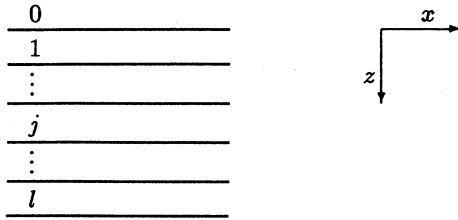


FIG. 1. Multilayer sample. Medium 0 is vacuum or air. The y direction is perpendicular to the plane of drawing.

finds for all j , $N_{jx} = \cos\psi$, where ψ is the angle of incidence. Hence the z component of \mathbf{N}_j (i.e., perpendicular to the interface) is

$$N_{jz} = (\epsilon_j - \cos^2\psi)^{1/2}. \quad (1)$$

That is,

$$N_{jz}'^2 = \frac{1}{2} \{ \epsilon_j' - \cos^2\psi + [(\epsilon_j' - \cos^2\psi)^2 + \epsilon_j''^2]^{1/2} \}, \quad (2)$$

$$N_{jz}'' = \epsilon_j'' / (2N_{jz}'), \quad (3)$$

$$N_j' = (\cos^2\psi + N_{jz}'^2)^{1/2}. \quad (4)$$

The angle of ψ_j of \mathbf{N}_j' with the interface is given by

$$\tan\psi_j = N_{jz}' / N_{jx}' = N_{jz}' / \cos\psi. \quad (5)$$

Furthermore, one can write $N_{jz}' = N_j' \sin\psi_j \approx \sin\psi_j$, since $N_j' \approx 1$ (see Appendix A).

If there is no absorption ($\epsilon_j'' = 0$), Snell's law $n_0 \cos\psi = n_j \cos\psi_j$ is valid. Then total reflection will take place if the angle of incidence is less than the critical angle $\psi_c = \arcsin(1 - \epsilon_j')^{1/2} \approx (2\delta_j)^{1/2}$.

For s polarization (electric field parallel to the interface), the complex coefficients of reflection r_j and of transmission t_j , being the ratio of electric fields at the $j, j+1$ interface, are given by Fresnel's formulas

$$r_j = (N_{jz} - N_{j+1,z}) / (N_{jz} + N_{j+1,z}), \quad (6)$$

$$t_j = (2N_{jz}) / (N_{jz} + N_{j+1,z}). \quad (7)$$

In Appendix B the case of p polarization (magnetic field parallel to the interface) will be considered. In most practical cases, both give the same answer.

For rough interfaces the above formulas are no longer exact. Several methods are known to incorporate roughness.²⁸ In a well-known method, r_j is multiplied by a factor S_j (resembling a Debye-Waller factor), which is a function of the root-mean-square deviation σ_j of the interface atoms from the perfectly smooth situation. However, such expressions are only valid for small roughness ($2\pi\sigma_j |N_{jz}| / \lambda < 1$). Otherwise, the phase relation between incident and reflected beams is lost and hardly any specular reflection takes place. This is discussed further in Sec. II C.

There exist several expressions²⁸ for S_j , yielding identical results for ψ far above ψ_c . An expression (derived using a vector model^{29,30}), which gives good results (also for $\psi \lesssim \psi_c$), is

$$S_j = \exp[-2(2\pi\sigma_j / \lambda)^2 N_{jz} N_{j+1,z}], \quad (8)$$

whereas t_j has to be multiplied by $\exp[(2\pi\sigma_j / \lambda)^2 (N_{jz} - N_{j+1,z})^2 / 2]$.

In a second method, which is also valid for intermediate roughness, the rough transition layer between two materials is approximated by a series of layers in which the dielectric constant varies slowly.²⁸

Up to now, reflection and refraction at a single interface were considered. In a multiple thin-film sample, the electric fields throughout the material can be found either from a matrix formalism^{18,23} or, equivalently, from a recursion relation.^{5,31}

B. Energy flow and absorption in a single layer

In this section energy flow through a single interface will be considered; the case of a multilayer sample will be treated in Sec. II C.

It is well known²³ that the time-averaged energy flux, i.e., the energy flowing through a unit surface area per unit time, is given by the Poynting vector

$$\mathbf{P}_j = \frac{1}{2} \text{Re}(\mathbf{E}_j \times \mathbf{H}_j^*) = \frac{1}{2} \text{Re}(\mathbf{E}_j^* \times \mathbf{H}_j). \quad (9)$$

For s polarization one finds

$$\mathbf{P}_j = \frac{|E_j|^2}{2Z_0} \mathbf{N}_j', \quad (10)$$

where $Z_0 = (\mu_0 / \epsilon_0)^{1/2}$ is the impedance of vacuum. Hence, for s polarization, \mathbf{P}_j is parallel to \mathbf{N}_j' and the angle of energy flow θ_j , i.e., the angle of \mathbf{P}_j with the interface, is

$$\theta_j = \psi_j. \quad (11)$$

For p polarization this is no longer true exactly, though it is in good approximation (see Appendix B). The magnitude of \mathbf{P}_j is approximately $P_j \approx |E_j|^2 / (2Z_0)$ for both polarization directions (see Appendixes A and B).

The position dependence of \mathbf{P}_j is found by substituting the plane-wave expression in Eq. (10):

$$\mathbf{P}_j = \frac{|E_j^t|^2 \mathbf{N}_j'}{2Z_0} \exp\left[-\frac{4\pi N_{jz}'' z}{\lambda}\right], \quad (12)$$

where E_j^t is the electric field at the top of layer j (i.e., at $z=0$). Using Eq. (3), one finds

$$\mathbf{P}_j = \frac{|E_j^t|^2 \mathbf{N}_j'}{2Z_0} \exp\left[-\frac{2\pi \epsilon_j'' z}{\lambda N_{jz}'}\right]. \quad (13)$$

Now the connection can be made with the linear absorption coefficient $\mu_{j\lambda}$ (the mass absorption coefficient times the density). This is defined at perpendicular incidence ($\psi=90^\circ$), in which case the attenuation factor is given by $\exp(-\mu_{j\lambda} z)$. So

$$\begin{aligned} \mu_{j\lambda} &= \frac{2\pi \epsilon_j''}{\lambda N_{jz}'(\psi=90^\circ)} \\ &= \frac{2\pi \epsilon_j''}{\lambda} \left[\frac{1}{2} [\epsilon_j' + (\epsilon_j'^2 + \epsilon_j''^2)^{1/2}] \right]^{-1/2}. \end{aligned}$$

From this one finds

$$\epsilon_j'' = \frac{\lambda \mu_{j\lambda}}{2\pi} \left[\epsilon_j' + \frac{\lambda^2 \mu_{j\lambda}^2}{16\pi^2} \right]^{1/2}. \quad (14)$$

Making the small δ_j and small β_j approximation (Appendix A), $\epsilon_j'' \approx \lambda \mu_{j\lambda} / (2\pi)$. With $N_{jz}' \approx \sin\psi_j$, Eq. (13) becomes

$$\mathbf{P}_j \approx \frac{|E_j'|^2 \mathbf{N}_j'}{2Z_0} \exp \left[-\frac{\mu_{j\lambda} z}{\sin\psi_j} \right].$$

This formula, with the exponential decay described by the absorption coefficient, has the expected form.²⁸ Note, however, that some approximations have been made which are not valid in the soft x-ray regime ($\lambda \gtrsim 10$ nm; see Appendix A).

This has also been investigated by Henke.⁶ He defines an extinction coefficient $\kappa_j \equiv \epsilon_j'' / (2N_j')$ and writes the attenuation factor [in the text preceding his Eq. (33)] in terms of the angle of energy flow θ_j as

$$\exp[-4\pi\kappa_j z / (\lambda \sin\theta_j)] = \exp[-2\pi\epsilon_j'' z / (\lambda N_j' \sin\theta_j)].$$

However, from Eq. (13) above it can be seen that the correct expression is $\exp[-2\pi\epsilon_j'' z / (\lambda N_j' \sin\psi_j)]$. So, in contrast to Henke's⁶ statement, the factor is the same for *s* and *p* polarization. Fortunately, most of his considerations remain valid. For hard x rays, $\kappa_j \approx \beta_j$, and for soft x rays, Henke makes a comparison between κ_j and β_j , and also between the refraction angles θ_j and the reflectivities for the two polarizations (cf. Appendix B). His conclusion is that for Al *Kα* (0.874 nm), the differences are very small, but for Be *Kα* (11.38 nm), the differences can be rather large, as can be expected from the considerations in Appendix A.

Next, the absorption of radiation in the material will be considered. According to Poynting's theorem, the amount of electromagnetic energy absorbed per unit time within a volume bounded by a surface *S* can be described by

$$A = - \int \int_S \mathbf{P}_j \cdot \mathbf{u} \, ds,$$

where *ds* is an area element of *S* and \mathbf{u} is a unit vector perpendicular to *ds*. From this, the amount of energy absorbed by a slice of material at depth *z* with infinitesimal thickness *dz* and with top and bottom surface area both equal to S_1 is found to be $dA = [-P_{jz}(z+dz) + P_{jz}(z)]S_1$, neglecting the four sides with height *dz*. Expanding $P_{jz}(z+dz)$ up to first order in *dz* yields

$$dA = -S_1 \frac{\partial P_{jz}}{\partial z} dz. \quad (15)$$

So the amount of absorbed radiation is proportional to $-\partial P_{jz} / \partial z$.

From Eq. (12) [and (3)], one obtains, for *s* polarization,

$$-\frac{\partial P_{jz}}{\partial z} = \frac{|E_j'|^2}{2Z_0} \frac{2\pi\epsilon_j''}{\lambda} \exp \left[-\frac{4\pi N_{jz}'' z}{\lambda} \right], \quad (16)$$

which is in good approximation equal to

$$-\partial P_{jz} / \partial z \approx (|E_j'|^2 / 2Z_0) [\mu_{j\lambda} \exp(-\mu_{j\lambda} z / \sin\psi_j)].$$

For *p* polarization this equation also applies in good approximation (Appendix B).

The results derived here differ from those given by Lefèvre and Montel.²⁶ They suggest in their Sec. 4.7 that *dA* is proportional to $\exp[-4\pi N_{jz}'' / (\lambda \sin\theta_j)] dz / \sin\theta_j$. The $\sin\theta_j$ in the exponent seems to be a simple mistake. The second $\sin\theta_j$ can be justified, because it cancels with the $\sin\theta_j$ dependence of the flux density on the surface area S_1 .

Up to now, the effect of possible reflected radiation from the bottom interface of layer *j* has not been taken into account. This will be done in Sec. II C.

The number of absorbed photons per unit time is obtained from Eq. (15) by dividing by the incident photon energy hc / λ , where *h* is Planck's constant and *c* is the velocity of light in vacuum. Now the primary XRF intensity I_{aj} , i.e., the number of photons emitted per unit time by atoms of a particular element *a* in layer *j*, is obtained from the number of absorbed photons by integration over the layer thickness d_j multiplied by several factors: the fraction of absorbed radiation which is used for photoionization of the considered shell of atom *a*, the probability of emission of the considered radiation, and the absorption factors for the outgoing radiation. Hence

$$I_{aj} = \frac{\lambda}{hc} C_{aj} \frac{\tau_{a\lambda}}{\mu_{j\lambda} / \rho_j} J_{a\lambda} w_a g_a \exp \left[-\sum_{n=1}^{j-1} \frac{\mu_{na} d_n}{\sin\psi_d} \right] S_1 \times \int_0^{d_j} dz \left[-\frac{\partial P_{jz}}{\partial z} \right] \exp \left[-\frac{\mu_{ja} z}{\sin\psi_d} \right], \quad (17)$$

where C_{aj} is the mass fraction of element *a* in layer *j*, ρ_j is the density of material *j*, $\tau_{a\lambda}$ is the photoelectric part of the mass absorption coefficient for element *a* at wavelength λ , $J_{a\lambda}$ is the absorption jump factor at wavelength λ for the creation of holes in the considered shell of element *a*, w_a is the fluorescence yield for the decay of holes in the considered shell of *a*, g_a is the relative emission rate for the considered XRF line in preference to other lines originating from the same hole in *a*, and μ_{na} is the linear absorption coefficient of the considered fluorescence radiation from element *a* in layer *n*.³³ It is supposed that the detection angle ψ_d is far above the critical angle for total reflection of the outgoing radiation. Note that the attenuation of the incident radiation is already incorporated in P_{jz} (see above). I_{aj} is the total emitted intensity; dividing by 4π gives the emitted number of photons per unit time per unit solid angle. Equation (17) will be worked out further below.

The surface area S_1 is the irradiated detected sample area.³⁴ In general, it will be equal to the detected area S_d (which varies as $\sin\psi_d$ with the angle of detection), provided that S_d is wholly irradiated. If, however, the irradiated sample area is so small that it is the limiting factor, S_1 varies with the angle of incidence as $1/\sin\psi$. In practice, this will often be avoided in the glancing-incidence region. Note that in both cases it is supposed that the sample is large enough. If the sample size is the limiting factor, S_1 is equal to the sample surface area.

Finally, it can be remarked that the above theory also applies for glancing-incidence photoelectron spectroscopy, as performed by Henke.⁶ Then, in Eq. (17), the factors $w_a g_a$ are not present, whereas for μ_{na} , etc. one has to substitute the linear electron attenuation coefficient (i.e., reciprocal mean free path) of the considered photoelectrons in layer n .

C. Energy flow and absorption in multiple thin films

With the knowledge from the previous sections, it is possible to calculate the total-energy flow and absorption within each layer of a multiple thin-film sample.

For s polarization the electric field is in the y direction. The total field at a point of \mathbf{r} in layer j is the sum of a transmitted contribution E_j^\downarrow and a reflected contribution E_j^\uparrow :

$$\mathbf{E}_j = \mathbf{E}_j^\downarrow + \mathbf{E}_j^\uparrow, \quad (18)$$

where

$$E_j^\downarrow = E_j^f \exp \left[-i \frac{2\pi}{\lambda} N_{jz} z \right] \exp \left[i \left[\omega t - \frac{2\pi}{\lambda} N'_{jx} x \right] \right], \quad (19)$$

$$E_j^\uparrow = E_j^r \exp \left[i \frac{2\pi}{\lambda} N_{jz} z \right] \exp \left[i \left[\omega t - \frac{2\pi}{\lambda} N'_{jx} x \right] \right], \quad (20)$$

and E_j^f and E_j^r are the transmitted and reflected fields at the top of layer j .³¹

Using Maxwell's equation $\nabla \times \mathbf{E}_j = -\mu_0 \partial \mathbf{H}_j / \partial t$ (where μ_0 is the vacuum permeability), one finds from Eqs. (18)–(20), for the components of the magnetic field H_j in layer j ,

$$\begin{aligned} H_{jx} &= \frac{1}{Z_0} (-E_j^\downarrow + E_j^\uparrow) N_{jz}, \\ H_{jy} &= 0, \\ H_{jz} &= \frac{1}{Z_0} (E_j^\downarrow + E_j^\uparrow) N'_{jx}. \end{aligned} \quad (21)$$

So the components of the Poynting vector are

$$\begin{aligned} P_{jx} &= \frac{1}{4} E_{jy}^* H_{jz} + \text{c.c.} = \frac{1}{2Z_0} |E_j^\downarrow + E_j^\uparrow|^2 \cos \psi, \\ P_{jy} &= 0, \\ P_{jz} &= -\frac{1}{4} E_{jx}^* H_{jz} + \text{c.c.} \\ &= \frac{1}{4Z_0} (E_j^\downarrow + E_j^\uparrow)^* (E_j^\downarrow - E_j^\uparrow) N_{jz} + \text{c.c.}, \end{aligned} \quad (22)$$

where c.c. denotes the complex conjugate of the preceding. Using Eqs. (19) and (20), Eq. (22) becomes

$$\begin{aligned} P_{jz} &= \frac{1}{2Z_0} \left\{ N'_{jz} |E_j^f|^2 \exp \left[-\frac{4\pi N'_{jz} z}{\lambda} \right] \right. \\ &\quad - N'_{jz} |E_j^r|^2 \exp \left[\frac{4\pi N'_{jz} z}{\lambda} \right] \\ &\quad \left. + N'_{jz} \left[i E_j^{f*} E_j^r \exp \left[\frac{4\pi i N'_{jz} z}{\lambda} \right] + \text{c.c.} \right] \right\}. \quad (23) \end{aligned}$$

The last term is due to interference between incoming and reflected radiation. Note, furthermore, that now the angle of energy flow, θ_j , depends on z . It is given by $\tan \theta_j = P_{jz} / P_{jx}$.

Up to now, this treatment is equivalent to that given by Król, Sher, and Kao.¹⁸ They give examples of calculations of P_j and θ_j and of fluorescence yields. The present formalism, however, is more general, and absorption and fluorescence enhancement can be incorporated in a relatively easy way.

According to Eqs. (15) and (17), the amount of absorbed radiation and the XRF intensity are proportional to $-\partial P_{jz} / \partial z$. From Eq. (23) one finds

$$\begin{aligned} -\frac{\partial P_{jz}}{\partial z} &= \frac{1}{2Z_0} \frac{4\pi}{\lambda} N'_{jz} N''_{jz} \left\{ |E_j^f|^2 \exp \left[-\frac{4\pi N'_{jz} z}{\lambda} \right] \right. \\ &\quad + |E_j^r|^2 \exp \left[\frac{4\pi N'_{jz} z}{\lambda} \right] \\ &\quad \left. + \left[E_j^{f*} E_j^r \exp \left[\frac{4\pi i N'_{jz} z}{\lambda} \right] \right. \right. \\ &\quad \left. \left. + \text{c.c.} \right] \right\}. \quad (24) \end{aligned}$$

Defining

$$A_{j1} = \frac{2\pi \epsilon_j''}{\lambda \mu_{j\lambda}} \frac{|E_j^f|^2}{|E_0|^2}, \quad (25)$$

$$A_{j2} = \frac{2\pi \epsilon_j''}{\lambda \mu_{j\lambda}} \frac{|E_j^r|^2}{|E_0|^2}, \quad (26)$$

$$A_{j3} = \frac{2\pi \epsilon_j''}{\lambda \mu_{j\lambda}} \frac{2E_j^{f*} E_j^r}{|E_0|^2}, \quad (27)$$

$$b_{j1} = 4\pi N'_{jz} / \lambda, \quad (28)$$

$$b_{j2} = -b_{j1}, \quad (29)$$

$$b_{j3} = -4\pi i N'_{jz} / \lambda, \quad (30)$$

Eq. (24) can be written as

$$-\frac{\partial P_{jz}}{\partial z} = \frac{|E_0|^2}{2Z_0} \mu_{j\lambda} \text{Re} \left[\sum_{m=1}^3 A_{jm} \exp(-b_{jm} z) \right]. \quad (31)$$

In the expressions for A_{jm} , using Eq. (14), one can put

$$2\pi \epsilon_j'' / (\lambda \mu_{j\lambda}) = [\epsilon_j' + \lambda^2 \mu_{j\lambda}^2 / (16\pi^2)]^{1/2} \approx 1.$$

For p polarization, similar expressions are found (Appendix B), and for both polarization directions, $-\partial P_{jz} / \partial z \approx \mu_{j\lambda} |E_j^\downarrow + E_j^\uparrow|^2 / (2Z_0)$. The XRF intensity now can be found from Eq. (17):

$$I_{aj} = I_0 C_{aj} \rho_j \tau_{a\lambda} J_{a\lambda} \omega_a g_a S_1 \exp \left[- \sum_{n=1}^{j-1} \frac{\mu_{na} d_n}{\sin \psi_d} \right] \times \operatorname{Re} \left\{ \sum_{m=1}^3 A_{jm} \int_0^{d_j} dz \exp \left[- \left(b_{jm} + \frac{\mu_{ja}}{\sin \psi_d} \right) z \right] \right\},$$

$$I_{aj} = I_0 C_{aj} \rho_j \tau_{a\lambda} J_{a\lambda} \omega_a g_a S_1 \exp \left[- \sum_{n=1}^{j-1} \frac{\mu_{na} d_n}{\sin \psi_d} \right] \times \operatorname{Re} \left[\sum_{m=1}^3 A_{jm} \frac{1 - \exp[-(b_{jm} + \mu_{ja}/\sin \psi_d) d_j]}{b_{jm} + \mu_{ja}/\sin \psi_d} \right] \quad (32)$$

where $I_0 = |E_0|^2 \lambda / (2Z_0 hc)$ is the number of incident photons per unit surface area per unit time. Integration yields

(where only the $m = 3$ term is complex).

For very thin layers (i.e., all exponents containing d_j small), this equation can be written

$$I_{aj} \approx \frac{1}{2Z_0 hc} \frac{2\pi\epsilon_j''}{\mu_{j\lambda}} C_{aj} \rho_j \tau_{a\lambda} J_{a\lambda} \omega_a g_a S_1 \exp \left[- \sum_{n=1}^{j-1} \frac{\mu_{na} d_n}{\sin \psi_d} \right] |E_j^i + E_j^r|^2 d_j.$$

Then the intensity is proportional to $C_{aj} \rho_j d_j$, i.e., the amount of element a in layer j .

The results for p polarization are given in Appendix B. Except for soft x rays, the results are the same for both polarization directions and the above equations for s polarization can be used.

From Eq. (32) the XRF intensity can be found, if E_j^i and E_j^r are calculated according to the method outlined above. A similar procedure has been suggested by Brunel and Gilles,¹⁵ who, however, simply state that the absorption is proportional to $|E_j^i + E_j^r|^2$, which is only approximately true for p polarization.

Interface roughness can be accounted for by the methods described in Sec. II A. For very rough interfaces, however, as, for instance, a granular residue on a flat substrate, there is a large spread in incident angles. In that case, if the high roughness concerns the $j-1, j$ interface, one can put $r_{j-1} \approx 0$, $t_{j-1} \approx 1$, $N'_{jz} \approx N'_{j-1,z}$, and

$$a_j \approx \exp \{ - [2\pi i \sin \psi_{j-1} / \lambda + \mu_{j\lambda} / (2 \sin \psi_{j-1})] d_j \}.$$

Moreover, for a granular residue in general, large thickness variations ($\gtrsim \lambda / [2\pi \sin \psi_{j-1}]$) are present. Then

there is no fixed phase relation between incoming and reflected beam, implying that the last (interference) term in the above equations vanishes and intensities have to be summed instead of fields.

D. Fluorescence enhancement

Up to now, only primary fluorescence, directly caused by the incident beam, was considered. It is well known³⁵⁻³⁸ in XRF that enhancement of the fluorescence emitted by atoms a is possible because of excitation by fluorescence radiation (with energy above the involved absorption edge of a) emitted by other atoms b in the sample. In most cases it is sufficient to take into account secondary fluorescence and to neglect higher-order processes.

In a multilayer both *intra-* and *interlayer* enhancement have to be considered. For instance, the interlayer secondary fluorescence caused by (a particular line of) element b in layer k , contributing to the considered fluorescence of element a in layer j below k , can be written as (cf. Refs. 37 and 38)

$$I_{aj}^{(bk)} = \frac{\lambda}{hc} C_{bk} \frac{\tau_{b\lambda}}{\mu_{k\lambda}/\rho_k} J_{b\lambda} \omega_b g_b C_{aj} \tau_{ab} J_{ab} \omega_a g_a \exp \left[- \sum_{n=1}^{j-1} \frac{\mu_{na} d_n}{\sin \psi_d} \right] S_1$$

$$\times \frac{1}{2} \int_0^{\pi/2} \tan \alpha \, d\alpha \int_0^{d_j} dz_a \int_0^{d_k} dz_b \left[- \frac{\partial P_{kz}}{\partial z_b} \right] \exp \left[- \frac{\mu_{ja} z_a}{\sin \psi_d} \right]$$

$$\times \exp \left[- \left(\mu_{kb} (d_k - z_b) + \sum_{n=k+1}^{j-1} \mu_{nb} d_n + \mu_{jb} z_a \right) / \cos \alpha \right] \quad (k < j), \quad (33)$$

where τ_{ab} is the photoelectric part of the mass absorption coefficient for element a at the wavelength of the considered fluorescence radiation emitted by b , and J_{ab} is the absorption jump factor at that wavelength for the creation of holes in the considered shell of element a . Similar expressions can be written down for $k > j$ and for $k = j$.

In these expressions the integration over all angles α at which the radiation can be emitted from an atom b is rather nasty. In the literature three methods are known to perform it. Mantler³⁷ uses numerical integration. This method, however, leads to unacceptably long computation times for a multilayer with several tens of layers. Rössiger³⁹ replaces the integration by a summation over three carefully selected angles. It is found that his method fails in the case of the very thin layers encountered here, which can be understood because his selection criterion does not involve such small distances. The present author³⁸ evaluated the integrals analytically, leading to expressions in terms of the exponential-integral function. These can be evaluated fast numerically. The complete expressions are given in Appendix C.

In the approach mentioned, no reflection and refraction of the fluorescence radiation were taken into account. One can question this approximation: For the very thin layers encountered here, the contribution to Eq. (33) from radiation emitted at small angles will be appreciable, whereas one can expect that in reality radiation emitted at $\alpha > \pi/2 - \psi_c$ will hardly contribute to inter-layer secondary fluorescence, because it is totally reflected. To obtain a feeling for this effect, for some of the cases discussed below the integration over α was performed numerically with an upper limit of $\pi/2 - \psi_c$. It was found that in all cases the relative error in the secondary contribution is never much more than 10%, in a total contribution of less than 10%. Thus the approximation made by neglecting this effect is considered reasonable.

E. Summary of computational method

With the formalism mentioned, the angular dependence of GIXF intensities from multilayer samples can be calculated. As input, one uses the wavelength λ and for each layer j the following: thickness d_j ; interface roughness σ_j ; density ρ_j ; mean atomic number (or scattering factor) Z_j ; mean atomic mass M_j ; mass fraction C_{aj} of detected element a ; mass absorption coefficients for incident and detected radiation, $\mu_{j\lambda}/\rho_j$ and μ_{ja}/ρ_j ; and for enhancement due to element b , mass absorption coefficients μ_{jb}/ρ_j and factors $\tau_{b\lambda}J_{b\lambda}w_b g_b \tau_{ab}J_{ab}/(\tau_{a\lambda}J_{a\lambda})$.³³ Furthermore, for rough interfaces one can choose from three possibilities: use of the "Debye-Waller factor" (as described in Sec. II A), varying dielectric constant, e.g., approximated by a variation in a few layers, or very rough interface without interference (see Sec. II C).

In general, the incident x rays will be hard enough to make the approximation that s and p polarizations give the same answer. Then it is possible to calculate for each layer ϵ_j [Eq. (14) and Ref. 27]; then, as a function of the angle of incidence ψ , N_{jz} [Eq. (1)], reflection coefficient r_j

[Eq. (6) times Debye-Waller factor S_j , Eq. (8)], and transmission coefficient t_j ; next all E_j^r and E_j^t are calculated;³¹ then the primary intensity can be calculated from Eq. (32) and the secondary contribution from Appendix C, which has to be summed over all layers k and all fluorescence lines of elements b with energy above the involved absorption edge of a . In most cases it is possible to take together the enhancement due to all lines originating from the same shell.^{33,36}

Finally, in order to compare with experiment, the intensity-*versus*- ψ curves can be convoluted by a divergent incident beam profile.

III. EXAMPLES OF CALCULATIONS

To illustrate the potentialities of glancing-incidence x-ray fluorescence, in this section some interesting theoretical examples will be given, whereas in the next section a comparison with experiments will be made. In all examples, Mo $K\alpha$ ($\lambda = 0.0711$ nm) is used for the incident radiation. Furthermore, it is supposed that the surface area from which XRF is detected is smaller than the irradiated area.

Figures 2 and 3 deal with a 70-nm-thick silicon layer on a gold substrate and Figs. 4 and 5 with a 1 nm Co/10 nm Au double layer on a silicon substrate. In the last example, the reflecting properties of the gold layer are hardly affected by the cobalt surface layer, which, however, can serve as a surface probe. In Figs. 2 and 4, both the reflectivity and XRF intensity (normalized at the value at high angles) are shown as a function of the glancing angle of incidence. In Figs. 3 and 5 the normalized incident intensity $|E_j^i + E_j^r|^2/|E_0|^2$ is drawn as a function of depth in the sample. Note that the negative depth values at the left correspond to the vacuum (or air) above the surface, whereas the right part corresponds to the first few nanometers of the substrate.

In the reflectivity, a region with nearly total reflection is seen for $\psi < \psi_c$ ($= 1.8$ mrad for Si and 4.6 mrad for

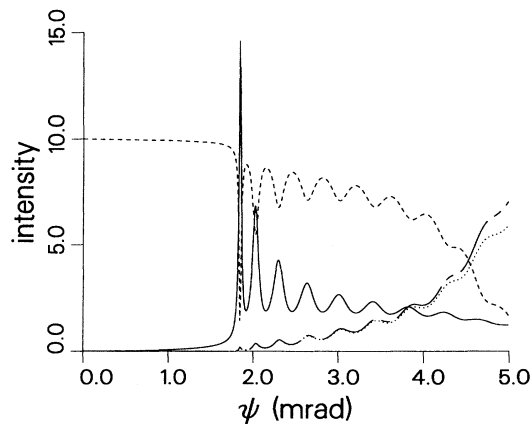


FIG. 2. (Normalized) intensity vs angle of incidence for 70 nm Si on Au: (10 \times) reflectivity (dashed line), Au $L\alpha$ (interrupted line), total Si $K\alpha$ (solid line), and (300 \times) contribution to Si $K\alpha$ due to secondary fluorescence from Au L and M lines (dotted line).

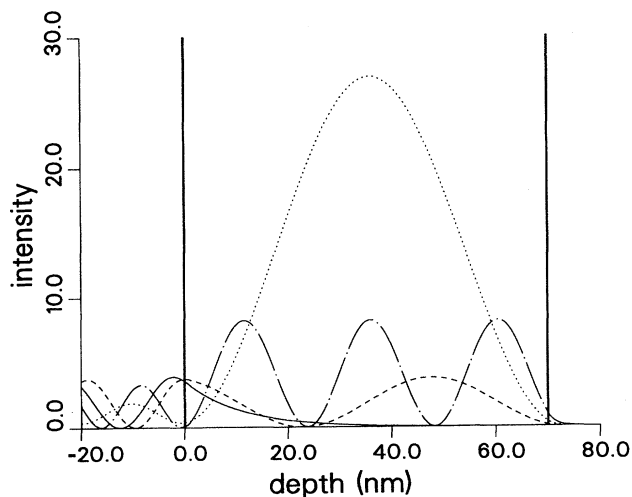


FIG. 3. (Normalized) intensity of incident x rays vs depth at $\psi=1.70$ (solid line), 1.85 (dotted line), 1.92 (dashed line), and 2.30 mrad (dot-dashed line) for vacuum/70 nm Si/Au. Interfaces are indicated by vertical lines.

Au), whereas for $\psi > \psi_c$ fringes are present as a result of interference between the transmitted and reflected radiation in the layer on the substrate.^{2,5} The position of the interference minima is given by $n\lambda = 2dN'_z$ [$\approx 2d \sin\psi(1 - \delta_j/\sin^2\psi)$ if $\psi \gg \psi_c$]. Above the surface a standing wave is present as a result of interference of incident and reflecting radiation,²² with a periodicity $\lambda/2\psi$ and a maximal amplitude of 4 times the incident intensity. In the material there is an evanescent wave for $\psi < \psi_c$, which can only excite a small XRF signal.¹³ For $\psi = \psi_c$ the intensity at the surface is 4, and so the maximum XRF intensity due to a thin surface layer is 4 times the value at high angle.

For a thicker layer, however, much higher intensity

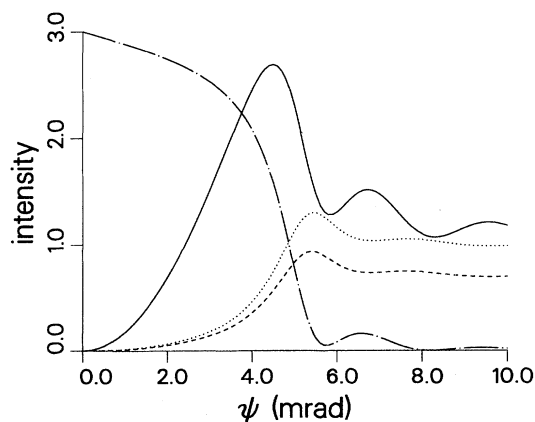


FIG. 4. (Normalized) intensity vs angle of incidence for 1 nm Co on 10 nm Au on Si: ($3\times$) reflectivity (dot-dashed line), Au $L\alpha$ (dotted line), total Co $K\alpha$ (solid line) and ($100\times$) contribution of Co $K\alpha$ due to secondary fluorescence from Au L line (dashed line).

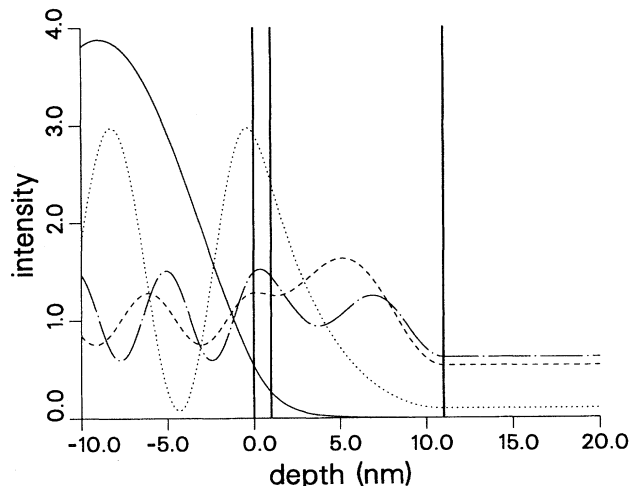


FIG. 5. (Normalized) intensity of incident x rays vs depth at $\psi=1.5$ (solid line), 4.5 (dotted line), 5.8 (dashed line) and 6.7 mrad (dot-dashed line) for vacuum/1 nm Co /10 nm Au/Si. Interfaces are indicated by vertical lines.

values can be reached. As far as is known, this effect has not been reported before.⁴⁰ At angles corresponding with reflectivity minima, a standing wave is formed which exactly fits between the two interfaces and the layer acts as a waveguide in which the radiation is pushed back and forth. In Fig. 3 the first and third resonance are shown for 70 nm silicon on gold. The first resonance takes place at $\psi=1.85$ mrad, just above ψ_c , with a maximum amplitude, halfway into the layer, of 27. Integrated over the whole layer, this yields an XRF intensity of 14 (Fig. 2). In this case the effect is large because the reflectivity just above ψ_c is high at both interfaces, whereas the absorption is small in the light material silicon. These two conditions are not met for Au $L\alpha$ in the gold-on-silicon case (Figs. 4 and 5): The absorption is rather high, and moreover, the first maximum occurs well above ψ_c , where the reflectivity is much smaller. For silicon on gold, the higher-order resonances are smaller too, because the reflectivity is smaller at higher ψ . In Fig. 2 the Au $L\alpha$ intensity is also shown. It exhibits small oscillations, because a small amount of the radiation from the silicon layer "leaks" into the substrate.

In Fig. 4 the XRF intensity is shown of both the cobalt surface layer and the thicker gold layer. It is clear that the two give a completely different angular behavior: in the reflectivity minima, the intensity at the surface is minimal, as is the surface-layer XRF, whereas the intensity in the gold layer and XRF signal from it is close to maximal. Note that the cobalt can be considered as a surface layer because its thickness is small, compared to both the evanescent-wave penetration and standing-wave period.

In Figs. 2 and 4 also the enhancement due to secondary fluorescence excited by Au L and M lines is shown (on an enlarged scale), a contribution which does not exceed a few percent. It has approximately the same behavior as the Au $L\alpha$ fluorescence. There are small differences, be-

cause the upper part of the gold layer contributes relatively more to secondary fluorescence (mainly emission at small angles) than to primary fluorescence (measured at high emission angle).

Next, the influence of interface roughness will be discussed. Figure 6 deals with the same situation as Fig. 5, but with a surface roughness $\sigma=1.5$ nm at the gold-silicon interface. Because of the smaller reflectivity at this interface, the interference in the gold layer has diminished. In the model used, the reflectivity at each interface has been multiplied by a factor which changes the amplitude. This results in a discontinuity which, of course, does not occur in reality. A more realistic model is that of a transition layer with a varying dielectric constant, which, however, leads to more time-consuming calculations. It was found that a transition-layer thickness of about 3σ gives results which agree well with the other model. In Fig. 6 the case of $\psi=5.8$ mrad has been calculated by both methods. Indeed, a good agreement is found outside the transition layer. In Fig. 8 the XRF intensity calculated by both methods will be compared.

The following example concerns a periodic multilayer. If one period consists of two layers 1 and 2 with thicknesses d_1 and d_2 , in the reflectivity curve diffraction peaks occur at a position given by Bragg's law (including refraction and absorption): $n\lambda=2(d_1N'_{1z}+d_2N'_{2z})$. As is well known from dynamical diffraction theory,⁴¹ during diffraction, a standing wave is set up in the material. The antinode position of this wave changes over one unit-cell distance in passing the diffraction peak. This fact is used in x-ray standing wave XRF (Refs. 41 and 42) to determine atomic positions in a unit cell. The phenomenon has also been reported for multilayers.⁴ In Fig. 7 this is demonstrated for a multilayer consisting of 20 periods of 1.5 nm Co+2 nm Au on silicon. In the upgoing flank of the diffraction peak, the antinode of the standing wave is in the cobalt layers, giving a maximum in Co $K\alpha$ and a minimum in Au $L\alpha$, whereas in the downgoing flank the

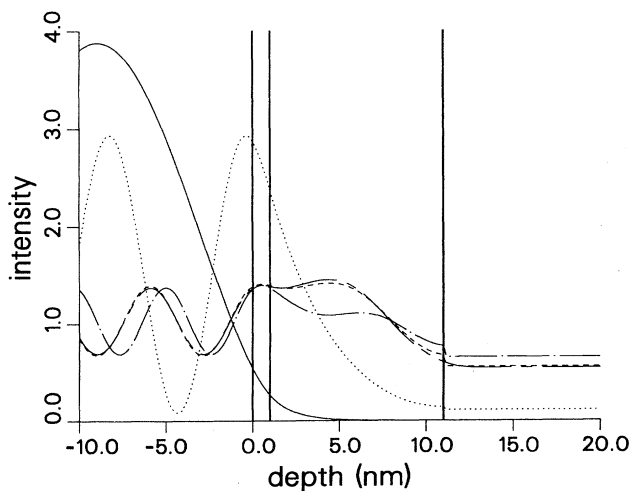


FIG. 6. *Idem* as Fig. 5, but with $\sigma=1.5$ nm at the Au/Si interface. Interrupted line: $\psi=5.8$ mrad, using transition-layer model (4.5 nm thick).

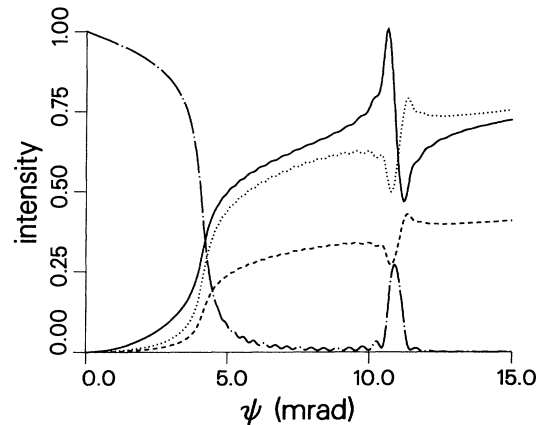


FIG. 7. (Normalized) intensity vs angle of incidence for 20 periods of 1.5 nm Co+2 nm Au on Si: Reflectivity (dot-dashed line), Au $L\alpha$ (dotted line), total Co $K\alpha$ (solid line), and (20 \times) contribution to Co $K\alpha$ due to secondary fluorescence from Au L lines (dashed line).

situation is reversed. Furthermore, the enhancement of Co $K\alpha$ due to secondary fluorescence by Au L lines is shown. As before, the effect approximately follows Au $L\alpha$ and does not exceed a few percent.

IV. COMPARISON WITH EXPERIMENT

In this section a comparison is made with illustrative experimental data²⁵ obtained with an instrument which is, in principle, a standard diffractometer equipped with an energy-dispersive system for XRF detection.¹⁹

In Fig. 8 the measured Co $K\alpha$ and Au $L\alpha$ intensities are shown for a sample consisting of 1 nm cobalt on 10

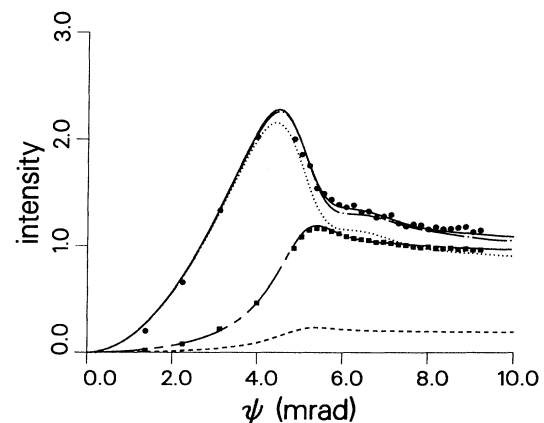


FIG. 8. (Normalized) intensity vs angle of incidence for 1 nm Co / 10 nm Au with 1% Co / Si: Measured Co $K\alpha$ (circles) and Au $L\alpha$ (squares) compared with calculations using $\sigma_{\text{Au/Si}}=1.8$ nm: Au $L\alpha$ (interrupted line), total Co $K\alpha$ (solid line), and Co $K\alpha$ from cobalt layer (dotted line) and from gold layer (dashed line). Dot-dashed line: Co $K\alpha$ calculated with transition-layer model (5 nm thick).

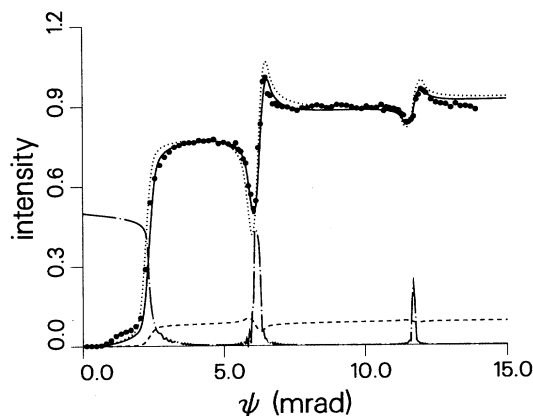


FIG. 9. (Normalized) Ni $K\alpha$ intensity vs angle of incidence for multilayer consisting of 50 periods of 1.6 nm Ni + 4.6 nm C on Si. Measured points (circles) compared with calculations using $\sigma=0.3$ nm at all interfaces; no Ni in C (dotted line), total intensity (solid line), and contribution from carbon layers (dashed line) for 10% Ni in the carbon layers. Dot-dashed line ($0.5\times$) reflectivity.

nm gold evaporated on a silicon substrate. Comparison with Fig. 4 shows that the maxima are less pronounced than in the calculation where perfectly smooth interfaces were assumed. It was found that with a gold-silicon interface roughness $\sigma=1.8$ nm the measured oscillations are reproduced. (As discussed above, a transition layer with thickness 5 nm gives approximately the same results.) However, the measured Co $K\alpha$ intensity above the gold critical angle is about 10% higher than that calculated (dotted line). Above, it was shown that secondary fluorescence caused by Au L lines is too small to explain this. However, a good fit is obtained by assuming that in the gold layer ~ 1 mass % cobalt is present, implying that more than 15% of the cobalt layer has dissolved into the gold layer. Indeed, Auger depth profiling after removal of the cobalt layer by chemical etching⁴³ showed that the gold layer contains an appreciable amount of cobalt.⁴⁴

Another example is shown in Fig. 9, which deals with a periodic multilayer consisting of 50 periods of 1.6 nm nickel and 4.6 nm carbon on silicon. From reflectivity measurements²⁵ it was found that all interfaces have a roughness $\sigma=0.3$ nm. In the measured Ni $K\alpha$ intensity, clearly the expected x-ray standing-wave behavior is seen at the first and second Bragg peak. With the above values, rather good agreement with experiment is found (dotted line). However, there is some discrepancy, especially in the extrema. Probably a small amount of nickel has dissolved into the carbon layers, for which the expected XRF (dashed line) has a maximum, where nickel has a minimum and vice versa. Indeed, a better fit was found (solid line) with the assumption that the carbon layer contains 10 mass % nickel; i.e., $\sim 7\%$ of the nickel has dissolved into the carbon layer.

From these examples it is seen that GIXF can be a useful tool for the investigation of the composition of layered materials.

V. DISCUSSION AND CONCLUSION

From the work done up to now, it is clear that a wealth of possibilities exists for GIXF.

For $\psi < \psi_c$ the penetration depth of the incident radiation is small. The resulting small background makes it possible in conventional total-reflection XRF (Ref. 10) to analyze very small quantities of material on top of flat substrates. The achieved detection limits are below 1 pg or 10^{10} atoms cm^{-2} for the first-row transition metals.⁴⁵

The standing wave above the surface has been used as a yardstick for distances in molecules adsorbed at the surface, both in the case of $\psi < \psi_c$ (Ref. 22) and at Bragg reflection from a multilayer.²¹ Up to now, no use has been made of the standing waves above the surface of a single layer on a substrate for $\psi > \psi_c$, which are both amplitude and frequency modulated (cf. Figs. 3 and 5).

Inside the material there is an evanescent wave with a highly angularly dependent penetration depth. This fact can be used to obtain information on depth distributions, e.g., of impurities in semiconductors.^{15,16} However, since the change in penetration depth takes place in a very narrow angular range, in practice the applicability of this effect for depth profiling is limited.

The situation is far more promising for layered materials, in which clear differences in dielectric constant are present. From the examples discussed in this paper, it can be concluded that GIXF is an interesting technique to obtain information on the depth distribution of elements in such materials: For periodic multilayers the shape of the GIXF intensity near a Bragg peak is rather sensitive to a change in composition, whereas for materials consisting of only a few layers the shape of the GIXF interference fringes can be used. It is striking that in the latter case the intensity of the incident x rays in a layer can be several tens of times higher than outside the material. This implies that GIXF is very sensitive to impurities at positions coinciding with standing-wave antinodes.

So the prospects for depth profiling of layered materials with GIXF are very good. One has to be aware, however, that the interpretation of the measurements depends for a great deal on modeling. The certainty of the interpretation can be increased if several GIXA measurements are combined. In the examples of Sec. IV, this was done in the first example by using both Co $K\alpha$ and Au $L\alpha$, and in the second example by using both reflectivity and Ni $K\alpha$.

In Table I, GIXF is compared to other techniques. Other GIXA techniques are not included, because they have worse detection limits (although for specific problems they may be preferable). GIXF is the only nondestructive technique which is able to give information with such a good depth resolution and such good detection limits. As in GIXF measurements have to be done above ψ_c , the detection limits are worse than those mentioned above for TXRF. The analyzed surface area is rather large, which, depending on the problem, might be either an advantage or a disadvantage. The typical depth resolution in GIXF of 1 nm is valid for a material consisting of distinct layers with a thickness of some nanometers. In other cases other techniques may be more suitable.

TABLE I. Comparison of different techniques for analysis of layered materials: depth resolution, analyzed surface area, lower limit of detection (LLD) (for first-row transition metals in silicon), and destructiveness of glancing-incidence x-ray fluorescence, conventional x-ray fluorescence, electron-probe microanalysis (EPMA), Rutherford backscattering spectrometry (RBS), transmission electron microscopy combined with energy-dispersive x-ray analysis (TEM/EDX), scanning Auger electron spectroscopy (AES), secondary-ion-mass spectroscopy (SIMS), and (provided that specific etchants are available) chemical etching combined with furnace atomic absorption spectroscopy.

Technique	Depth resolution (cm)	Area (cm ²)	LLD (atoms cm ⁻²)	Destructive?
GIXF	10 ⁻⁷	10 ⁰	10 ¹²	no
XRF	10 ⁻⁵	10 ⁰	10 ¹³	no
EPMA	10 ⁻⁵	10 ⁻⁸	10 ¹⁴	no
RBS	10 ⁻⁶	10 ⁻³	10 ¹³	no
TEM/EDX	10 ⁻⁶	10 ⁻¹²	10 ¹⁵	yes
AES	10 ⁻⁶	10 ⁻⁹	10 ¹²	yes
SIMS	10 ⁻⁶	10 ⁻⁵	10 ⁹	yes
chem. etch	10 ⁻⁸	10 ⁰	10 ¹¹	yes

However, for molecular-beam epitaxially and chemical vapor deposition grown materials, metallization and dielectric layers in integrated-circuit technology, magnetic multilayers, soft-x-ray monochromators, and many other layered materials, GIXF can yield chemical and structural information which is not easily obtained by other methods.

ACKNOWLEDGMENTS

This work was done in fruitful collaboration with W. W. van den Hoogenhof (Philips Analytical), who performed the experiments described in Sec. IV. A. J. G. Leenaers did the measurements on the cobalt-gold double layer on silicon, which was provided by Dr. W. Hoving. The chemical etching of cobalt was performed by A. Huizing and the Auger analysis by W. M. van de Wijgert.

APPENDIX A: APPROXIMATIONS

Here the approximations which are valid for small δ_j and small β_j are discussed. One can consider four cases, depending on the magnitude of $\epsilon'_j - \cos^2\psi \approx \sin^2\psi - 2\delta_j$. From Eqs. (2) and (4) one finds the following:

for $\epsilon'_j - \cos^2\psi \gg 2\delta_j$,

$$N_{jz}^{\prime 2} \approx \sin^2\psi - 2\delta_j + O(\beta_j^2), \quad N'_j \approx 1 - \delta_j + O(\beta_j^2) \approx 1;$$

for $|\epsilon'_j - \cos^2\psi| = O(\delta_j)$,

$$N_{jz}^{\prime 2} = O(\delta_j), \quad N'_j \approx 1 + O(\delta_j) \approx 1;$$

for $|\epsilon'_j - \cos^2\psi| \leq O(\beta_j)$,

$$N_{jz}^{\prime 2} = O(\beta_j), \quad N'_j \approx 1 + O(\beta_j) \approx 1;$$

for $\epsilon'_j - \cos^2\psi \ll 2\delta_j$,

$$N_{jz}^{\prime 2} \approx \beta_j^2 / 2\delta_j, \quad N'_j \approx 1 + O(\beta_j^2 / \delta_j) \approx 1.$$

The errors in the approximations are large only for

very soft x rays. For $\lambda = 10$ nm, $\delta_j = O(0.01)$, $\beta_j = O(10^{-7} \mu_{j\lambda} / \rho_j) \lesssim O(0.01)$. So, in general, for $\lambda \gtrsim 10$ nm the exact formulas have to be used.

APPENDIX B: *p* POLARIZATION AND OTHER POLARIZATION STATES

In Sec. II the theory was given for *s* polarization. Here the formulas for *p* polarization will be presented.

Fresnel's Eq. (6) becomes

$$r_j = \frac{N_{jz} / \epsilon_j - N_{j+1,z} / \epsilon_{j+1}}{N_{jz} / \epsilon_j + N_{j+1,z} / \epsilon_{j+1}},$$

for the reflection coefficient in terms of magnetic fields, and $t_j = 1 + r_j$.

In the small δ_j, β_j approximation, the formulas are the same for both polarizations: $N_{jz} / \epsilon_j \approx N_{jz}$, because

$$\text{Re}(N_{jz} / \epsilon_j) \approx N'_{jz} (1 + 2\delta_j + 2\beta_j^2 / N_{jz}^{\prime 2}) \approx N'_{jz}$$

and

$$-\text{Im}(N_{jz} / \epsilon_j) \approx N''_{jz} (1 + 2\delta_j - 2N_{jz}^{\prime 2}) \approx N''_{jz}.$$

Strictly speaking, the last equation is only valid if $|\epsilon'_j - \cos^2\psi| \ll 1$, but if this does not hold, in general, $N_{jz} \approx N_{j+1,z}$ and thus $r_j \approx 0$. The situation may be more complicated for soft x rays and if layer $j+1$ is much denser than layer j .

The Poynting vector [Eq. (9)] becomes, instead of Eq. (10),

$$\mathbf{P}_j = \frac{1}{2} \mathbf{Z}_0 |H_j|^2 \text{Re}(\mathbf{N}_j / \epsilon_j).$$

The angle of energy flow, θ_j , is given by $\tan\theta_j = P_{jz} / P_{jx}$. So, for *p* polarization, instead of Eq. (11),

$$\begin{aligned} \tan\theta_j &= \frac{\epsilon'_j N'_{jz} + \epsilon''_j N''_{jz}}{\epsilon'_j \cos\psi} \\ &= \tan\psi_j \left[1 + \frac{\epsilon''_j{}^2}{2\epsilon'_j N_{jz}^{\prime 2}} \right], \end{aligned}$$

where in the last step Eq. (5) has been used. Hence, approximately,

$$\tan\theta_j \approx \tan\psi_j(1 + 2\beta_j^2/N_{jz}'^2) \approx \tan\psi_j.$$

The magnitude of \mathbf{P}_j is

$$\begin{aligned} P_j &= \frac{1}{2} Z_0 |H_j|^2 \operatorname{Re} \left[\frac{N_j}{\epsilon_j} \right] \\ &= \frac{1}{2} Z_0 |H_j|^2 \frac{\cos\psi}{\cos\theta_j} \operatorname{Re} \left[\frac{1}{\epsilon_j} \right]. \end{aligned}$$

Furthermore, one can write $|E_j|^2 \approx Z_0^2 |H_j|^2$, using Appendix A. With $\cos\theta_j \approx \cos\psi$ and $\operatorname{Re}(1/\epsilon_j) \approx 1$, one finds $P_j \approx |E_j|^2 / (2Z_0)$.

The position dependence of \mathbf{P}_j is given by the same exponential factor as in Eq. (12). So

$$P_{jz} = \frac{1}{2} Z_0 |H_j^t|^2 \operatorname{Re}(N_{jz}/\epsilon_j) \exp(-4\pi N_{jz}''z/\lambda),$$

and instead of Eq. (16) one obtains

$$-\frac{\partial P_{jz}}{\partial z} = \frac{1}{2} Z_0 |H_j^t|^2 \operatorname{Re} \left[\frac{N_{jz}}{\epsilon_j} \right] \frac{4\pi N_{jz}''}{\lambda} \exp \left[-\frac{4\pi N_{jz}''z}{\lambda} \right],$$

or, approximately,

$$-\frac{\partial P_{jz}}{\partial z} \approx \frac{|E_j^t|^2}{2Z_0} \mu_{j\lambda} \exp \left[-\frac{\mu_{j\lambda} z}{\sin\psi_j} \right].$$

For p polarization Eqs. (18)–(20) are replaced by

$$\begin{aligned} \mathbf{H}_j &= \mathbf{H}_j^\downarrow + \mathbf{H}_j^\uparrow, \\ H_j^\downarrow &= H_j^t \exp \left[-i \frac{2\pi}{\lambda} N_{jz} z \right] \exp \left[i \left[\omega t - \frac{2\pi}{\lambda} N_{jx}' x \right] \right], \\ H_j^\uparrow &= H_j^r \exp \left[i \frac{2\pi}{\lambda} N_{jz} z \right] \exp \left[i \left[\omega t - \frac{2\pi}{\lambda} N_{jx}' x \right] \right], \end{aligned}$$

where H_j^t and H_j^r are calculated from $H_0 (= E_0/Z_0)$ in the same way³¹ as E_j^t and E_j^r from E_0 . From Maxwell's equation $\nabla \times \mathbf{H}_j = \epsilon_0 \epsilon_j \partial \mathbf{E}_j / \partial t$, one finds, for the components of the electric field,

$$E_{jx} = Z_0 (H_j^\downarrow - H_j^\uparrow) \frac{N_{jz}}{\epsilon_j},$$

$$E_{jy} = 0,$$

$$E_{jz} = Z_0 (-H_j^\downarrow - H_j^\uparrow) \frac{N_{jx}}{\epsilon_j}.$$

So the components of the Poynting vector are [instead of Eqs. (22) and (23)]

$$P_{jx} = -\frac{1}{4} E_{jz} H_{jy}^* + \text{c. c.} = \frac{1}{2} Z_0 |H_j^\downarrow + H_j^\uparrow|^2 \cos\psi \operatorname{Re}(1/\epsilon_j),$$

$$P_{jy} = 0,$$

$$\begin{aligned} P_{jz} &= \frac{1}{4} E_{jx} H_{jz}^* + \text{c. c.} = \frac{1}{4} Z_0 (H_j^\downarrow - H_j^\uparrow)(H_j^\downarrow + H_j^\uparrow)^* (N_{jz}/\epsilon_j) + \text{c. c.} \\ &= \frac{1}{2} Z_0 \{ \operatorname{Re}(N_{jz}/\epsilon_j) |H_j^t|^2 \exp(-4\pi N_{jz}''z/\lambda) - \operatorname{Re}(N_{jz}/\epsilon_j) |H_j^r|^2 \exp(4\pi N_{jz}''z/\lambda) \\ &\quad - \operatorname{Im}(N_{jz}/\epsilon_j) [i H_j^t H_j^r \exp(4\pi N_{jz}''z/\lambda) + \text{c. c.}] \}. \end{aligned}$$

In the calculation of $-\partial P_{jz}/\partial z$, one obtains, instead of Eqs. (25)–(27),

$$\begin{aligned} A_{j1} &= \frac{4\pi}{\lambda \mu_{j\lambda}} N_{jz}'' \operatorname{Re} \left[\frac{N_{jz}}{\epsilon_j} \right] \frac{|H_j^t|^2}{|H_0|^2}, \\ A_{j2} &= \frac{4\pi}{\lambda \mu_{j\lambda}} N_{jz}'' \operatorname{Re} \left[\frac{N_{jz}}{\epsilon_j} \right] \frac{|H_j^r|^2}{|H_0|^2}, \\ A_{j3} &= -\frac{4\pi}{\lambda \mu_{j\lambda}} N_{jz}' \operatorname{Im} \left[\frac{N_{jz}}{\epsilon_j} \right] \frac{2H_j^t H_j^r}{|H_0|^2}, \end{aligned}$$

and Eqs. (28)–(32) remain valid.

Above it was shown that in good approximation $\operatorname{Re}(N_{jz}/\epsilon_j) \approx N_{jz}'$, whereas $-\operatorname{Im}(N_{jz}/\epsilon_j) \approx N_{jz}''$ provided that $|\epsilon_j' - \cos^2\psi| \ll 1$. In general, if the last inequality is not true, H_j^r will be small, because r_j is small (see above), and A_{j2} and A_{j3} can be neglected. Furthermore, from the discussion above it follows that the ratio of the magnetic fields for p polarization is approximately the same as the ratio of electric fields for s polarization. So, in the small δ_j, β_j approximation the results for both polarization directions are identical. If this does not apply, the exact equations given here can be used.

For other polarization directions, P_{jy} no longer vanishes, and as was pointed out by Lefèvre and Montel,²⁶ the energy flow is no longer in the plane of incidence. However, because $N_{jy} = 0$, P_{jz} can be found from the y components of the electric field (E_j^\downarrow and E_j^\uparrow) and magnetic field (H_j^\downarrow and H_j^\uparrow) in a simple way, by adding the expressions given for s and p polarization:

$$P_{jz} = \frac{1}{4Z_0}(E_j^\downarrow + E_j^\uparrow)^*(E_j^\downarrow - E_j^\uparrow)N_{jz} + \frac{1}{4}Z_0(H_j^\downarrow - H_j^\uparrow)(H_j^\downarrow + H_j^\uparrow)^*\frac{N_{jz}}{\epsilon_j} + \text{c.c.},$$

where the y components of the fields can be found by the method outlined in Sec. II and above, if E_0 is substituted by $E_0 \cos \eta$ and H_0 by $E_0 \sin \eta / Z_0$, where η is the angle between the incident electric field E_0 and the y axis. In the same way, $-\partial P_{jz} / \partial z$ and I_{aj} are obtained by adding the expressions given for s and p polarization. For unpolarized radiation, the intensities are simply given by one-half the sum of the intensities for s and p polarization.

APPENDIX C: EXPRESSIONS FOR SECONDARY FLUORESCENCE

The interlayer secondary fluorescence caused by (a particular line of) element b in layer k contributing to the considered fluorescence of element a in layer j is found by substitution in Eq. (24) in equations such as Eq. (33) and integration:

$$\begin{aligned} I_{aj}^{(bk)} &= \frac{1}{2} I_0 C_{bk} \rho_k J_{b\lambda} \omega_b g_b \tau_{b\lambda} \tau_{ab} C_{aj} J_{ab} \omega_a g_a S_1 \exp \left[- \sum_{n=1}^j \mu_{na} d_n / \sin \psi_d \right] \\ &\quad \times \text{Re} \left[\sum_{m=1}^3 A_{km} X(b_{km}, \mu_{ja} / \sin \psi_d) \right] \quad (\text{for } k > j), \\ I_{aj}^{(bk)} &= \frac{1}{2} I_0 C_{bk} \rho_k J_{b\lambda} \omega_b g_b \tau_{b\lambda} \tau_{ab} C_{aj} J_{ab} \omega_a g_a S_1 \exp \left[- \sum_{n=1}^{j-1} \mu_{na} d_n / \sin \psi_d \right] \\ &\quad \times \text{Re} \left[\sum_{m=1}^3 A_{km} \exp(-b_{km} d_k) X(-b_{km}, -\mu_{ja} / \sin \psi_d) \right] \quad (\text{for } k < j), \\ I_{aj}^{(bj)} &= \frac{1}{2} I_0 C_{bj} \rho_j J_{b\lambda} \omega_b g_b \tau_{b\lambda} \tau_{ab} C_{aj} J_{ab} \omega_a g_a S_1 \exp \left[- \sum_{n=1}^{j-1} \mu_{na} d_n / \sin \psi_d \right] \\ &\quad \times \text{Re} \left[\sum_{m=1}^3 A_{jm} [Q(b_{jm}, \mu_{ja} / \sin \psi_d) + Q(\mu_{ja} / \sin \psi_d, b_{jm})] \right] \quad (\text{for } k = j), \end{aligned}$$

where

$$X(p, q) = V(d_j, d_k) - V(d_j, 0) - V(0, d_k) + V(0, 0),$$

with

$$\begin{aligned} V(d_j, d_k) &= \exp \left[(q - \mu_{jb}) d_j - (p + \mu_{kb}) d_k - \sum_n \mu_{nb} d_n \right] \\ &\quad \times \left[\frac{\mu_{kb}}{p(p\mu_{jb} + q\mu_{kb})} D \left[\left(1 + \frac{p}{\mu_{kb}} \right) \left[\mu_{jb} d_j + \sum_n \mu_{nb} d_n + \mu_{kb} d_k \right] \right] \right. \\ &\quad \left. + \frac{\mu_{jb}}{q(p\mu_{jb} + q\mu_{kb})} D \left[\left(1 - \frac{q}{\mu_{jb}} \right) \left[\mu_{jb} d_j + \sum_n \mu_{nb} d_n + \mu_{kb} d_k \right] \right] - \frac{1}{pq} D \left[\mu_{jb} d_j + \sum_n \mu_{nb} d_n + \mu_{kb} d_k \right] \right], \end{aligned}$$

where the summation over n is from $n = j + 1$ to $k - 1$ for $k > j$ and from $n = k + 1$ to $j - 1$ for $k < j$. If $\sum_n \mu_{nb} d_n = 0$,

$$V(0, 0) = - \frac{1}{p\mu_{jb} + q\mu_{kb}} \left[\frac{\mu_{kb}}{p} \ln \left| 1 + \frac{p}{\mu_{kb}} \right| + \frac{\mu_{jb}}{q} \ln \left| 1 - \frac{q}{\mu_{jb}} \right| \right].$$

Furthermore

$$\begin{aligned} Q(p, q) &= \exp[-p + \mu_{jb} d_j] \left[- \frac{1}{pq} D(\mu_{jb} d_j) + \frac{1}{q(p+q)} D((\mu_{jb} - q) d_j) + \frac{1}{p(p+q)} D((p + \mu_{jb}) d_j) \right] \\ &\quad + \frac{1}{p(p+q)} \ln \left| 1 + \frac{p}{\mu_{jb}} \right| + \frac{1}{q(p+q)} \exp[-(p+q) d_j] \ln \left| 1 - \frac{q}{\mu_{jb}} \right|. \end{aligned}$$

In the above equations, $D(x)$ is defined as

$$D(x) = \exp(x) E_1(x),$$

where $E_1(x)$ is the exponential-integral function⁴⁶

$$E_1(x) = \int_x^\infty dy \exp(-y)/y.$$

For real arguments this function can be evaluated rapidly using standard algorithms.⁴⁷ However, because b_{k3} is imaginary, in the interference terms the arguments are complex. If interference is appreciable, the imaginary part (of the order $b_{k3}d_k$) will be a few times π , whereas the real part (of the order $\mu_{kb}d_k$) is small. In that case, $D(x+iy)$ can be developed in a Taylor series around the imaginary part, yielding, up to third order,

$$D(x+iy) \approx \exp(x+iy)E_1(iy) + \frac{ix}{y} + \frac{1}{2}x^2 \left[\frac{i}{y} - \frac{1}{y^2} \right] + \frac{1}{6}x^3 \left[\frac{i}{y} - \frac{1}{y^2} - \frac{2i}{y^3} \right] \quad (\text{if } x \lesssim 0.1y),$$

with

$$E_1(iy) = -\text{Ci}|y| + i \frac{y}{|y|} \left[\text{Si}|y| - \frac{\pi}{2} \right].$$

The cosine integral $\text{Ci}(y)$ and sine integral $\text{Si}(y)$ (Ref. 46) can be evaluated by fast standard routines.⁴⁸

On the other hand, if the above approximation is not valid, A_{k3} will be so small that the complex term need not be calculated.

- ¹A. H. Compton and S. K. Allison, *X-Rays in Theory and Experiment* (Van Nostrand, New York, 1935).
- ²H. Kiessig, *Ann. Phys. (Leipzig)* **10**, 769 (1931).
- ³J. Du Mond and J. P. Youtz, *J. Appl. Phys.* **11**, 357 (1940).
- ⁴T. W. Barbee, Jr. and W. K. Warburton, *Mater. Lett.* **3**, 17 (1984).
- ⁵L. G. Parratt, *Phys. Rev.* **95**, 359 (1954).
- ⁶B. L. Henke, *Phys. Rev. A* **6**, 94 (1972).
- ⁷R. Barchewitz, M. Cremonese-Visicato, and G. Onori, *J. Phys. C* **11**, 4439 (1978); S. M. Heald, in *X-ray Absorption*, edited by D. C. Koningsberger and R. Prins (Wiley, New York, 1988), p. 87.
- ⁸W. C. Marra, P. Eisenberger, and A. Y. Cho, *J. Appl. Phys.* **50**, 6927 (1979); A. Segmüller, I. C. Noyan, and V. S. Speriosu, *Prog. Cryst. Growth Charact.* **18**, 21 (1989).
- ⁹Y. Yoneda and T. Horiuchi, *Rev. Sci. Instrum.* **42**, 1069 (1971).
- ¹⁰P. Wobrauschek, H. Aiginger, G. Owesny, and C. Strelj, *J. Trace Microprobe Techniq.* **6**, 295 (1988); A. Prange, *Spectrochim. Acta B* **44**, 437 (1989).
- ¹¹P. Eichinger, H. J. Rath, and H. Schwenke, in *ASTM STP 990*, edited by D. C. Gupta (American Society for Testing and Materials, Philadelphia, 1988), p. 305.
- ¹²V. Penka and W. Hub, *Spectrochim. Acta B* **44**, 483 (1989).
- ¹³R. S. Becker, J. A. Golovchenko, and J. R. Patel, *Phys. Rev. Lett.* **50**, 153 (1983).
- ¹⁴J. M. Bloch, *et al.*, *Phys. Rev. Lett.* **54**, 1039 (1985).
- ¹⁵M. Brunel, *Acta Crystallogr. A* **42**, 304 (1986); M. Brunel and B. Gilles, *J. Phys. (Paris) Colloq.* **50**, C7-85 (1989).
- ¹⁶A. Iida, K. Sakurai, A. Yoshinaga, and Y. Gohshi, *Nucl. Instrum. Methods A* **246**, 736 (1986); A. Iida, K. Sakurai, and Y. Gohshi, *Adv. X-Ray Anal.* **31**, 487 (1988).
- ¹⁷B. Lengeler, *Mikrochim. Acta* **1**, 455 (1987); *Adv. Mater.* **2**, 123 (1990).
- ¹⁸A. Król, C. J. Sher, and Y. H. Kao, *Phys. Rev. B* **38**, 8579 (1988).
- ¹⁹D. K. G. de Boer and W. W. van de Hoogenhof, *Spectrochim. Acta B* (to be published).
- ²⁰W. Berneike (unpublished); H. Schwenke (unpublished).
- ²¹M. J. Bedzyk *et al.*, *Science* **241**, 1788 (1988).
- ²²M. J. Bedzyk, G. M. Bommarito, and J. S. Schildkraut, *Phys. Rev. Lett.* **62**, 1376 (1989).
- ²³M. Born and W. Wolf, *Principles of Optics*, 5th ed. (Pergamon, Oxford, 1975).
- ²⁴H. Schwenke, W. Berneike, J. Knoth, and U. Weisbrod, *Adv. X-Ray Anal.* **32**, 105 (1989); J. Knoth, H. Schwenke, and U. Weisbrod, *Spectrochim. Acta B* **44**, 477 (1989).
- ²⁵D. K. G. Boer and W. W. van den Hoogenhof, *Adv. X-Ray Anal.* (to be published).
- ²⁶M.-R. Lefèvre and M. Montel, *C. R. Acad. Sci. B* **273**, 329 (1971); *Opt. Acta* **20**, 97 (1973).
- ²⁷The imaginary part of ϵ_j describes absorption [cf. Eq. (14)] whereas the real part is $\epsilon'_j = 1 - N_A r_e \lambda^2 \rho_j Z_j / (\pi M_j)$, where N_A is Avogadro's constant, r_e is the classical electron radius, ρ_j is the density of material j , M_j is the mean atomic mass of the material, and Z_j is the real part of the mean atomic scattering factor, which is equal to the mean atomic number if anomalous dispersion can be neglected. For a compound consisting of elements n , $Z_j = \sum_n C_{nj}^a Z_n$ and $M_j = \sum_n C_{nj}^a M_n$, where C_{nj}^a is the atomic fraction of element n in material j .
- ²⁸L. Névt and P. Croce, *Rev. Phys. Appl.* **15**, 761 (1980); *P. Croce, Acta Electron.* **24**, 247 (1981/1982).
- ²⁹B. Vidal and P. Vincent, *Appl. Opt.* **23**, 1794 (1984).
- ³⁰B. Pardo, T. Megademini, and J. M. André, *Rev. Phys. Appl.* **23**, 1579 (1988).
- ³¹In the recursive method the transmitted field E_j^t and reflected field E_j^r at the top of layer j are found from $E_j^t = a_j^2 X_j E_j^t$ and $E_{j+1}^r = a_j E_j^r t_j / (1 + a_{j+1}^2 X_{j+1} r_j)$, where $a_j = \exp(-2\pi i d_j N_{jz} / \lambda)$ (d_j is the thickness of layer j) and $X_j = (r_j + a_{j+1}^2 X_{j+1}) / (1 + a_{j+1}^2 X_{j+1} r_j)$. For the substrate, $X_l = 0$.
- ³²The penetration depth of the radiation can be defined from Eq. (13) as $l_j = \lambda N_{jz} / (2\pi \epsilon_j'')$. In good approximation this is $l_j \approx \sin \psi_j / \mu_{j\lambda}$. For $\psi \ll \psi_c$, $l_j \approx (\rho_j Z_j / M_j)^{-1/2} \times 3.4$ nm (with ρ_j in g cm^{-3}). In the neighborhood of ψ_c , l_j increases steeply, and for $\psi \gg \psi_c$, $l_j \approx \sin \psi / \mu_{j\lambda}$.
- ³³D. K. G. de Boer, *Spectrochim. Acta B* **44**, 1171 (1989).
- ³⁴D. K. G. de Boer, *X-Ray Spectrom.* **18**, 119 (1989).
- ³⁵J. Sherman, *Spectrochim. Acta* **7**, 283 (1955).
- ³⁶M. L. Verheijke and A. W. Witmer, *Spectrochim. Acta B* **33**, 817 (1978).
- ³⁷M. Mantler, *Anal. Chim. Acta* **188**, 25 (1986).
- ³⁸D. K. G. de Boer, *X-Ray Spectrom.* **19**, 145 (1990) [in this paper there is an error in Eq. (10b) which is corrected in Appen-

- dix C above].
- ³⁹V. Rössiger, *Isotopenpraxis* **21**, 417 (1985); **23**, 325 (1987); *X-Ray Spectrom.* **17**, 107 (1988); V. Rössiger and H.-J. Thomas, *ibid.* **19**, 211 (1990).
- ⁴⁰Lengeler (Ref. 17) reports a very high intensity for a thin layer; this is because of the factor $S_1 = 1/\sin\psi$, which is taken into account for a narrow incident beam.
- ⁴¹B. R. Batterman, *Phys. Rev.* **133**, A759 (1964); B. R. Batterman and H. Cole, *Rev. Mod. Phys.* **36**, 681 (1964).
- ⁴²J. R. Patel *et al.*, *J. Vac. Sci. Technol. B* **7**, 894 (1989).
- ⁴³The cobalt layer was selectively removed by a cerium (IV) nitrate-perchloric acid etch.
- ⁴⁴Auger depth profiling without chemical etching is not exclusive, because always intermixing during sputtering occurs. Furthermore, it was found that the cobalt concentration is higher in the upper part of the gold layer. However, this hardly affects the calculated GIXF results.
- ⁴⁵A. Prange (unpublished); M. Schuster, *Spectrochim. Acta B* (to be published).
- ⁴⁶*Handbook of Mathematical Functions*, Natl. Bur. Stand. Appl. Math. Ser. No. 55, edited by M. Abramowitz and I. Stegun (U.S. GPO, Washington, D.C., 1965), Chap. 5.
- ⁴⁷IMSL routine MMDEI (IMSL, Houston, 1984).
- ⁴⁸NAG routines S13ACF and S13ADF (Numerical Algorithms Group, Oxford, 1987).